

From Dia- to Paramagnetic Orbital Susceptibility of Massless Fermions

A. Raoux,^{1,3} M. Morigi,¹ J.-N. Fuchs,^{2,1,*} F. Piéchon,¹ and G. Montambaux¹

¹Laboratoire de Physique des Solides, CNRS UMR 8502, Université Paris-Sud, F-91405 Orsay, France

²Laboratoire de Physique Théorique de la Matière Condensée, CNRS UMR 7600, Université Pierre et Marie Curie, 4 place Jussieu, F-75252 Paris, France

³Département de Physique, École Normale Supérieure, 24 rue Lhomond, 75231 Paris Cedex 05, France

(Received 16 July 2013; published 14 January 2014)

We study the orbital susceptibility of multiband systems with a pair of Dirac points interpolating between honeycomb and dice lattices. Despite having the same zero-field energy spectrum, these different systems exhibit spectacular differences in their orbital magnetic response, ranging from dia- to paramagnetism at Dirac points. We show that this striking behavior is related to a topological Berry phase varying continuously from π (graphene) to 0 (dice). The latter strongly constrains interband effects, resulting in an unusual dependence of the magnetic response also at finite doping.

DOI: 10.1103/PhysRevLett.112.026402

PACS numbers: 71.10.Pm, 72.80.Vp, 73.22.Pr, 75.20.-g

Introduction.—Among the fascinating electronic properties of graphene, orbital magnetism is certainly one of the least studied experimentally [1]. This is due to the difficulty of measuring the magnetic response of such a thin solid [2]. Theoretically, it has long been known that undoped graphene should be strongly diamagnetic [3]. This behavior was attributed to the response of Dirac-Weyl fermions which properly describe the low energy electronic properties of graphene. Here, we show that another simple system also featuring massless fermions, the so-called dice (or \mathcal{T}_3) lattice [4,5], surprisingly presents a huge paramagnetic response in a magnetic field. These two systems have the same zero field energy spectrum [see Fig. 1(b)] but exhibit opposite magnetic behaviors (see Fig. 2) not only at zero doping but also in a whole energy range between the two van Hove singularities, where interband effects are important. To shed light on these surprising features, we study a lattice model which interpolates between graphene and dice lattices. We show that the continuous evolution of the magnetic response is associated to a Berry phase which, although being here a topological quantity, is no more quantized as in graphene, but varies continuously between π and 0.

The honeycomb (graphene) and the dice lattices are examples of electronic systems featuring coupled energy bands for which the Landau-Peierls (or single-band) approach [6] fails to obtain the orbital susceptibility χ . Here the band of itinerant electrons is made of two subbands touching at two Dirac points. In the case of graphene, by considering the vicinity of the Dirac points where the spectrum is linear, McClure showed that the magnetic field spectrum exhibits peculiar Landau levels (LLs) [3]. Neglecting the contribution of the rest of the band, he could derive a diamagnetic peak precisely at the Dirac point, i.e., for zero doping, where Landau-Peierls would predict a vanishing susceptibility. Later, Fukuyama developed a linear response formalism that takes interband

effects into account [7]. This formalism has recently been applied to the tight-binding model of graphene to calculate $\chi(\mu)$ where the chemical potential μ varies in the entire band [8]. The divergence of the susceptibility at $\mu = 0$ appears as a $\delta(\mu)$ peak, which is the signature of a nonanalytic behavior of the grand potential as a function of the magnetic field [9].

In order to get a better understanding of the fundamental reason for this peculiar behavior, we study a modified tight-binding model for spinless electrons hopping on the \mathcal{T}_3 lattice, which we call $\alpha\text{-}\mathcal{T}_3$. Starting from the honeycomb lattice with two sites (A, B) per unit cell and a hopping amplitude t , the \mathcal{T}_3 lattice is obtained by connecting additional (C) sites at the center of each hexagon to the B sites [see Fig. 1(a)] with a hopping amplitude αt . Depending on the real parameter α , this model interpolates between graphene ($\alpha = 0$) and the dice lattice ($\alpha = 1$). Its interest is that the zero field spectrum (within a trivial appropriate normalization) does not depend on α [see Fig. 1(b)], while the zero field wave functions and the finite field spectrum present a continuous evolution which

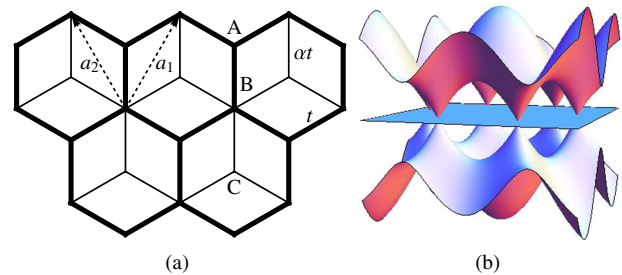


FIG. 1 (color online). $\alpha\text{-}\mathcal{T}_3$ model. (a) \mathcal{T}_3 lattice. Thick links: nearest neighbors hoppings t between A and B sites forming a honeycomb lattice. Thin links: additional hoppings αt connecting C to B sites. Varying α interpolates between the honeycomb lattice ($\alpha = 0$) and the dice lattice ($\alpha = 1$). (b) Zero field energy spectrum as a function of the wave vector \mathbf{k} for all α .

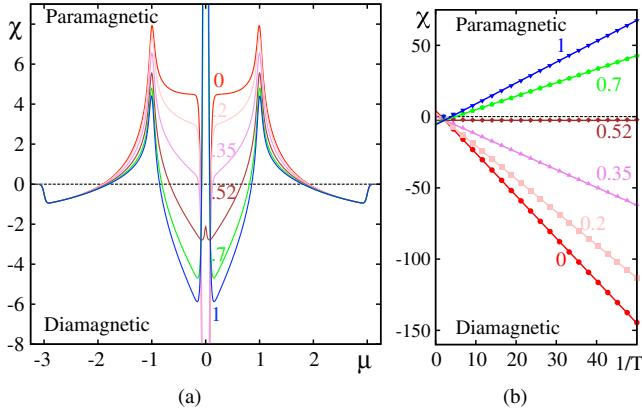


FIG. 2 (color online). (a) Numerically obtained orbital susceptibility χ [in units of the Landau band edge value $|\chi_L| = (1/16\pi)(e^2 t a^2 / \hbar^2)$] as a function of the chemical potential μ (in units of t) in the whole band for various α as indicated and for a temperature $T = 0.02t$. Because of a sum rule discussed below, the orbital response at zero doping is systematically compensated by an opposite response at finite doping. (b) Susceptibility peak at zero chemical potential as a function of the inverse temperature for various α [same units as in (a)]. The slope is well fitted by $-3\zeta_\gamma(2)/\zeta(2)$, in agreement with Eq. (11).

may be described by an α -dependent Berry phase. Then, we compute the low-energy LLs, from which we obtain the low field dependence of the magnetization. By considering different temperature limits, we explicitly show that the magnetic response continuously evolves from a diamagnetic to a paramagnetic behavior, when increasing α . We finally present simple arguments to explain this spectacular change of the orbital response, backup our low energy analytical results by numerical calculations on the full tight-binding model, show how the susceptibility is affected in the whole band, and suggest an experimental realization.

The α - \mathcal{T}_3 model.—We first introduce a convenient parametrization of α with the angle φ such that $\tan \varphi \equiv \alpha$. Because of the three sites per unit cell, the Bloch Hamiltonian reads (after rescaling the energy by $\cos \varphi$ [10]):

$$H(\mathbf{k}) = \begin{pmatrix} 0 & f_{\mathbf{k}} \cos \varphi & 0 \\ f_{\mathbf{k}}^* \cos \varphi & 0 & f_{\mathbf{k}} \sin \varphi \\ 0 & f_{\mathbf{k}}^* \sin \varphi & 0 \end{pmatrix}, \quad (1)$$

where $f_{\mathbf{k}} = -t(1 + e^{-ik \cdot \mathbf{a}_1} + e^{-ik \cdot \mathbf{a}_2})$, $\mathbf{a}_1 = a(\sqrt{3}/2, 3/2)$, and $\mathbf{a}_2 = a(-\sqrt{3}/2, 3/2)$ are Bravais lattice vectors [Fig. 1(a)], a is the intersite distance, and the wave vector $\mathbf{k} = (k_x, k_y)$. The model has a $\alpha \rightarrow 1/\alpha$ duality and we therefore restrict ourselves to $\alpha \in [0, 1]$. The corresponding spectrum is independent of α and consists of three bands, each of them carrying $1/3$ of the states: a zero-energy flat band $\epsilon_{k,0} = 0$ and two dispersive bands

$\epsilon_{k,\lambda} = \lambda|f_{\mathbf{k}}|$, with the band index $\lambda = \pm$, see Fig. 1(b). The latter are identical to the bands of graphene [1] and feature two inequivalent contact points at the corners $\pm\mathbf{K}$ of the hexagonal Brillouin zone, where $f(\pm\mathbf{K}) = 0$. To distinguish these two contact points, we introduce a valley index $\xi = \pm$. Close to zero energy, linearization near $\xi\mathbf{K}$ gives $f_{\mathbf{k}} \approx v(\xi q_x - iq_y)$ where the velocity $v \equiv 3ta/2$, $\mathbf{q} = \mathbf{k} - \xi\mathbf{K}$ and we have set $\hbar \equiv 1$. The low-energy spectrum is therefore $\epsilon_{q,0} = 0$ and $\epsilon_{q,\lambda} = \lambda v|\mathbf{q}|$ and electrons behave as massless fermions. The eigenvectors in the whole Brillouin zone read

$$|\psi_\lambda\rangle = \frac{1}{\sqrt{2}} \begin{pmatrix} \cos \varphi e^{i\theta_{\mathbf{k}}} \\ \lambda \\ \sin \varphi e^{-i\theta_{\mathbf{k}}} \end{pmatrix}, \quad |\psi_0\rangle = \begin{pmatrix} \sin \varphi e^{i\theta_{\mathbf{k}}} \\ 0 \\ -\cos \varphi e^{-i\theta_{\mathbf{k}}} \end{pmatrix}, \quad (2)$$

where $f_{\mathbf{k}} = |f_{\mathbf{k}}|e^{i\theta_{\mathbf{k}}}$ defines the angle $\theta_{\mathbf{k}}$ and $|\psi_0\rangle$ corresponds to the zero energy flat band. For any path encircling a single valley, the finite energy bands are characterized by a Berry phase $\phi_{\lambda,\xi} = \xi\pi \cos 2\varphi$, while the flat band has a Berry phase $\phi_{0,\xi} = -\xi 2\pi \cos 2\varphi \equiv \xi 4\pi \sin^2 \varphi$ (modulo 2π). Note that $\phi_{0,\xi} + \sum_\lambda \phi_{\lambda,\xi} = 0$, $\sum_\xi \phi_{\lambda,\xi} = 0$ and $\sum_\xi \phi_{0,\xi} = 0$ as it should. It is remarkable that, except for $\alpha = 0$ or 1 , the Berry phase $\phi_{\lambda,\xi}$ is different in the two valleys. To our knowledge, this is the first example where Berry phases are topological but not π quantized.

Dirac-Weyl Hamiltonians.—For $\alpha = 0$, the α - \mathcal{T}_3 model is simply that of graphene except for the additional zero energy flat band originating from the uncoupled C atoms. As this flat band is inert, we will refer to the 0 - \mathcal{T}_3 model as graphene, notwithstanding the three sites per unit cell. Close to each valley, the linearized Hamiltonian can be written in the Dirac-Weyl form $H_\xi = v(\xi q_x \sigma_x + q_y \sigma_y) \oplus 0$, where σ_x, σ_y are spin $1/2$ Pauli matrices [1].

For $\alpha = 1$, the α - \mathcal{T}_3 model is that of the usual dice lattice [4]. In the vicinity of the contact points, the Hamiltonian may be linearized in a Dirac-Weyl form as $H_\xi = v(\xi q_x S_x + q_y S_y)$, similar to graphene except that S_x, S_y are now spin 1 matrices [11]. The α - \mathcal{T}_3 model therefore provides a continuous interpolation between pseudospin $1/2$ ($\alpha = 0$) and pseudospin 1 ($\alpha = 1$) massless fermions. However, when $\alpha \neq 0, 1$, the model involves more than a single pseudospin operator.

Landau level spectrum.—We now add a perpendicular magnetic field B to study the evolution of the LL spectrum with α . To do so, we restrict ourselves to the vicinity of the contact points where the zero field spectrum is linear, that is in an energy interval $[-W, W]$ where W is a cutoff, typically smaller than t . Performing the usual Peierls substitution $q_x \pm iq_y \rightarrow \sqrt{2eB} \hat{a}^\dagger / \hat{a}$, that introduces ladder operators such that $[\hat{a}, \hat{a}^\dagger] = 1$, the low-energy Hamiltonian in the K valley becomes

$$H_+ = \epsilon_B \begin{pmatrix} 0 & \cos \varphi \hat{a} & 0 \\ \cos \varphi \hat{a}^\dagger & 0 & \sin \varphi \hat{a} \\ 0 & \sin \varphi \hat{a}^\dagger & 0 \end{pmatrix}, \quad (3)$$

where $\epsilon_B \equiv v\sqrt{2eB}$ is a characteristic magnetic energy. In the other (K') valley, H_- is obtained from H_+ by the substitution $\hat{a} \rightarrow -\hat{a}^\dagger$. The Landau spectrum in each valley is given by $\epsilon_{l,\xi} = \pm\epsilon_B\sqrt{l + \gamma_\xi}$, where $l \in \mathbb{N}$ is the Landau index and $\gamma_+ = \sin^2\phi = 1 - \gamma_-$ is a valley-dependent index shift. The latter is related to the above computed Berry phase $\phi_{\lambda,\xi}$ via the semiclassical relation $\gamma_\xi = 1/2 - \phi_{\lambda,\xi}/2\pi$, see, e.g., [12,13], which is here found to be exact. As γ_ξ depends on the valley index, we stress that the twofold valley degeneracy (a prominent property in graphene) is lifted for all levels by the magnetic field as soon as $\alpha \neq 0, 1$. In order to treat both valleys at once, it is convenient to relabel the LLs as

$$\epsilon_n \equiv \pm\epsilon_B\sqrt{|n + \gamma|}, \quad (4)$$

with $\gamma = \gamma_+$ and a new Landau index $n \in \mathbb{Z}$ that now also takes negative values. When $\alpha \neq 0, 1$, each LL ϵ_n has a degeneracy eB/h per unit area. LLs are plotted as a function of α in Fig. 3(a). For graphene ($\alpha = 0$), the Landau spectrum is $\epsilon_n = \pm\epsilon_B\sqrt{|n|}$, $n \in \mathbb{Z}$, including a zero energy LL [3]. For the dice lattice ($\alpha = 1$), it is given by $\epsilon_n = \pm\epsilon_B\sqrt{|n + 1/2|}$ [11].

For all α , in addition to the LLs, a zero-energy flat band of topological origin exists in an arbitrary magnetic field, carrying 1/3 of the states (for $\alpha = 1$, see [5]).

Magnetization of massless fermions.—In order to compute the orbital magnetization, we work in the grand canonical statistical ensemble and consider the low energy LL spectrum (4). The grand potential is written as $\Omega(\mu, T) = \int \mathcal{N}(\epsilon) f'_\mu(\epsilon) d\epsilon$, where $\mathcal{N}(\epsilon)$ is the doubly integrated density of states (DOS), measured from the bottom of the spectrum and $f'_\mu(\epsilon)$ is the Fermi-Dirac function with chemical potential μ and temperature $T = 1/\beta$ (with $k_B \equiv 1$) [14]. It is then convenient to write it as a function of the doubly integrated DOS $\mathcal{N}_0(\epsilon)$ measured from zero energy. Neglecting terms which are field independent, we find that the field dependent part $\delta\mathcal{N} \equiv \mathcal{N}(B) - \mathcal{N}(B = 0)$ can be written as $\delta\mathcal{N}(\epsilon) = \delta\mathcal{N}_0(\epsilon) - \delta\mathcal{N}_0(-W)$, where W is the energy cutoff (in the low field limit $W/\epsilon_B \rightarrow \infty$) [15]. The DOS (per unit area) in the vicinity of the contact points is given by

$$\nu(\epsilon, B) = \frac{eB}{h} \sum_{n,\pm} \delta(\epsilon \pm \epsilon_B\sqrt{|n + \gamma|}), \quad (5)$$

including both valleys. The contribution of the flat band, which is field independent, has been excluded. Using the Poisson formula, we rewrite the DOS as

$$\nu(\epsilon, B) = \frac{|\epsilon|}{\pi\hbar^2 v^2} \left| 1 + 2 \sum_{p=1}^{\infty} \cos \frac{2\pi p \epsilon^2}{\epsilon_B^2} \cos 2\pi p \gamma \right|. \quad (6)$$

After a double integration, we obtain $\mathcal{N}_0(\epsilon)$ and $\delta\mathcal{N}(\epsilon)$ [15]. Then, we find that the field dependent part of the grand potential (per unit area) is given by

$$\delta\Omega_\alpha(\mu, T) = rB^{3/2} \sum_{p=1}^{\infty} \frac{\cos 2\pi p \gamma}{p^{3/2}} \int_{-\infty}^{\infty} f'_\mu(\epsilon) \Delta \left(2\sqrt{p} \frac{|\epsilon|}{\epsilon_B} \right) d\epsilon, \quad (7)$$

where $r \equiv v e^{3/2} / (2\pi^2 \sqrt{2\hbar})$ and $\Delta(x) \equiv 1 - 2S(|x|)$ in terms of the Fresnel function $S(x)$. As we now show, the sign of the grand potential depends on the index shift γ .

First consider the low temperature $T \ll \epsilon_B$ limit. The thermal function $f'_\mu(\epsilon) \rightarrow -\delta(\epsilon - \mu)$ so that the grand potential becomes

$$\delta\Omega_\alpha(\mu, T = 0) = rB^{3/2} w_\alpha(\mu/\epsilon_B), \quad (8)$$

where the function $w_\alpha(x) \equiv \sum_{p=1}^{\infty} [\cos(2\pi p \gamma) / p^{3/2}] \times \Delta(2\sqrt{p}x)$, exhibiting de Haas-van Alphen oscillations, is plotted in Fig. 3(b). It generalizes the function calculated by McClure in the case of graphene $\alpha = 0$ (Fig. 3 of Ref. [3]). In the particular case $\mu = 0$, the magnetization $\mathcal{M}_\alpha = -\partial\delta\Omega_\alpha/\partial B$ is nonanalytic (for $\alpha = 0$, see [9])

$$\mathcal{M}_\alpha = C_\alpha \sqrt{B}, \quad \text{where } C_\alpha = -(3/2)\zeta_\gamma(3/2)r \quad (9)$$

and

$$\zeta_\gamma(n) \equiv \sum_{p=1}^{\infty} \frac{1}{p^n} \cos 2\pi p \gamma = \text{Re}[\text{Li}_n(e^{2i\gamma\pi})], \quad (10)$$

with $\text{Li}_n(z)$ the polylogarithm function [16]. The square root behavior (9) cannot be captured by linear response

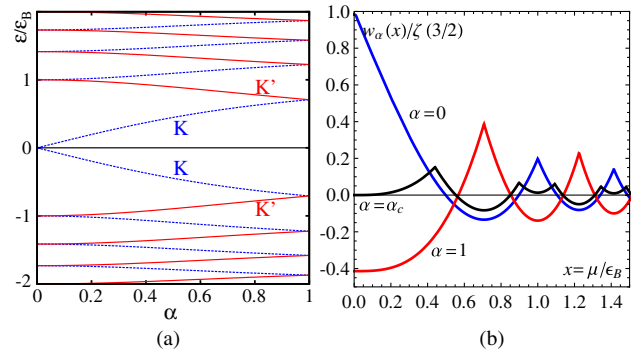


FIG. 3 (color online). (a) Landau level spectrum ϵ_n (each color corresponding to one valley) near zero energy as a function of the parameter α from graphene ($\alpha = 0$) to dice ($\alpha = 1$). (b) Function $w_\alpha(x)$ giving the dependence of the grand potential $\delta\Omega_\alpha$ (at finite magnetic field and zero temperature) on the chemical potential μ , see Eq. (8). Blue: graphene ($\alpha = 0$). Red: dice lattice ($\alpha = 1$). Black: critical case ($\alpha_c = 0.49065$).

approaches. A similar anomalous scaling $\mathcal{M} \propto \sqrt{B}$ was found for nodal fermions in [17]. For graphene ($\alpha = 0$, $\gamma = 0$), the prefactor is $C_0 = -(3/2)\zeta(3/2)r = -(3ve^{3/2}\zeta(3/2))/(4\pi^2\sqrt{2}\hbar) < 0$ [9]; whereas for dice ($\alpha = 1$, $\gamma = 1/2$), we find $C_1 = -C_0(\sqrt{2} - 1)/\sqrt{2} > 0$. Contrary to the case of graphene, the dice lattice is paramagnetic. This is confirmed numerically (see below) as shown in Fig. 2(b). More generally, $C_\alpha/|C_0|$ is plotted as a function of α as a full line in Fig. 4(b). The magnetization crosses over from dia- to paramagnetism when increasing α . The magnetization changes sign when $\alpha_c \approx 0.49065$, corresponding to $\gamma \approx 0.19403$. Duality $\alpha \rightarrow 1/\alpha$ implies $\mathcal{M}_{1/\alpha} = \mathcal{M}_\alpha$.

Second, at finite temperature $T \gg \epsilon_B$, on the scale of the thermal function, we can replace $\Delta(x)$ by $(4/\pi)\delta(x)$ so that Eq. (7) shows that the grand potential now varies like B^2 , which is the standard linear response behavior [14]. The susceptibility $-\partial^2\Omega/\partial B^2|_{B \rightarrow 0}$ is found to be

$$\chi_\alpha = \chi_0 \frac{\zeta_\gamma(2)}{\zeta(2)}, \quad \text{where } \chi_0 = -\frac{e^2 v^2}{12\pi T} \text{sech}^2\left(\frac{\beta\mu}{2}\right), \quad (11)$$

as found by McClure when $\alpha = 0$ [3] (spin degeneracy is not included here) and where $\zeta_\gamma(2)$ is defined in Eq. (10). In the $T \rightarrow 0$ limit (still with $T \gg \epsilon_B$), it can be written as $\chi_0 = -(e^2 v^2/3\pi)\delta(\mu)$. The sign change of χ_α occurs at $\alpha \approx 0.51764$, which is not exactly at the same value as for \mathcal{M}_α in the $T \ll \epsilon_B$ limit. Duality implies $\chi_{1/\alpha} = \chi_\alpha$.

Numerics.—We now consider the energy levels in a magnetic field for the infinite $\alpha\mathcal{T}_3$ lattice (Hofstadter

spectrum, see [5] for $\alpha = 1$ and [18] for $\alpha = 0$), and compute the grand potential numerically (see also [19]). First, at $T = 0$ and $\mu = 0$, we find that the magnetization \mathcal{M}_α is the sum of an anomalous $C_\alpha\sqrt{B}$ and a regular $D_\alpha B$ contribution [Fig. 4(a)]. The coefficients C_α and D_α are plotted in Fig. 4(b); C_α is properly given by Eq. (9). The α -dependent regular contribution $D_\alpha B$ is expected to come from interband contributions due to lattice effects beyond the massless fermions approximation. In that respect, a perturbative approach, such as that developed in [8] for $\alpha = 0$, might be helpful to quantitatively describe the fitted parameter D_α .

Next, we compute the finite temperature ($T \gg \epsilon_B$) susceptibility χ as a function of μ in the whole band for different values of α and for $T \ll t$ [Fig. 1(a)]. For $\alpha = 0$, aside from the central diamagnetic peak, we recover the $\chi(\mu)$ of [8]. For all α , we checked the following sum rule: the integral of the orbital susceptibility over the whole band $\int d\mu\chi(\mu)$ vanishes [15]. The α -dependent $\chi(\mu)$ is an indication of the importance of wave function dependent interband effects that affect not only the singularity at zero energy but also its behavior in a whole energy range, essentially between the two van Hove singularities. At $\mu = 0$, the susceptibility is a linear function of $1/T$ [Fig. 1(b)] with a slope which is well fitted by $-e^2 v^2 \zeta_\gamma(2)/[12\pi\zeta(2)]$ as predicted by Eq. (11). The slope changes sign from dia- to paramagnetic at $\alpha \approx 0.52$.

Discussion.—The physical origin of this dia- to paramagnetic crossover may be understood following usual textbook arguments. Figure 5 shows how the zero field spectrum coalesces into LLs for the cases of graphene and dice lattices. In the case of graphene, the contribution of each slice $[E_{n-1}, E_n]$, which condenses into the LL of energy ϵ_n , decreases the energy, and therefore gives a paramagnetic contribution. However, the contribution of the first (red) slice $[0, E_0]$, which condenses into the zero energy LL $\epsilon_0 = 0$, increases the energy and thus provides a diamagnetic contribution which actually compensates the total paramagnetic contribution of all other slices, giving a total diamagnetic contribution. For the dice lattice, the

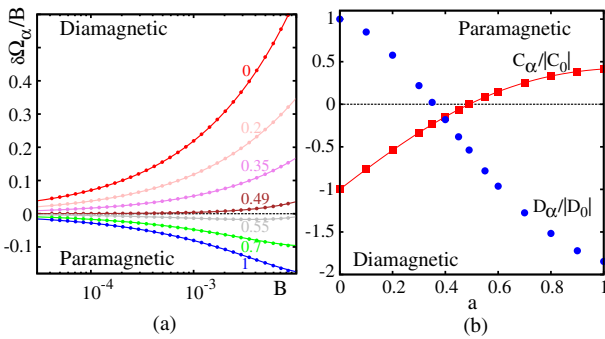


FIG. 4 (color online). (a) Field dependent part of the grand potential (per unit area) divided by the magnetic field $\delta\Omega_\alpha/B$ (in units of et/h), at zero doping $\mu = 0$ and temperature $T = 0$, as a function of the magnetic field B (in units of $(4\pi/\sqrt{3})(\hbar/ea^2)$) for various α as indicated. Dots are obtained numerically from the Hofstadter spectrum on the corresponding lattice: $\delta\Omega_\alpha/B$ is well fitted by a dependence $-(2/3)C_\alpha\sqrt{B} - (1/2)D_\alpha B$, corresponding to a magnetization $\mathcal{M}_\alpha = C_\alpha\sqrt{B} + D_\alpha B$. (b) Dimensionless parameters $C_\alpha/|C_0|$ and $D_\alpha/|D_0|$, obtained from the fit, as a function of α , with $C_0 = -(9\zeta(3/2)/8\pi^2\sqrt{2})(e^{3/2}ta/\hbar^{3/2})$ and $D_0 \approx 0.094(e^2ta^2/\hbar^2) \approx 4.7|\chi_L|$. Dots are numerical results and the full line is the analytical prediction Eqs. (9) and (10).

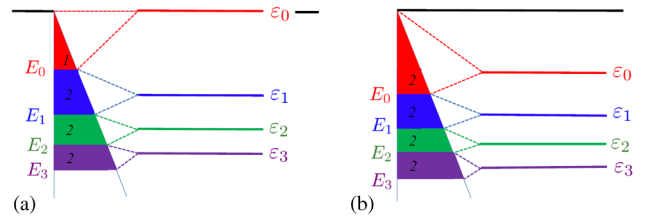


FIG. 5 (color online). Coalescence of the zero field spectrum (lower band near zero energy) into Landau levels ϵ_n . (a) Graphene ($\alpha = 0$): $\epsilon_n = -\sqrt{|n|}\epsilon_B$; $E_n = -\sqrt{n+1/2}\epsilon_B$ with $n \geq 0$. (b) Dice ($\alpha = 1$): $\epsilon_n = -\sqrt{|n+1/2|}\epsilon_B$; $E_n = -\sqrt{n+1}\epsilon_B$ with $n \geq 0$. The area of each colored slice $[E_{n-1}, E_n]$ counts the total number of states in this slice in zero field. In a field, these states condense into LL.

contribution of all slices (including the first) is paramagnetic, leading to a total paramagnetic contribution. Therefore, the contribution of the zero-energy LL is essential. In the intermediate case, the twofold degeneracy of the levels is lifted [Fig. 3(a)], the $n = 0$ LL acquires a finite energy; therefore, its contribution becomes less important. There is a continuous crossover between the two extreme cases represented in Fig. 5. The qualitative argument following this figure can, of course, be turned into a quantitative calculation of the grand potential, which reproduces the results obtained above.

Conclusion.—We have shown that the orbital susceptibility of a system featuring massless fermions can be continuously tuned from dia- to paramagnetic as a function of a hopping parameter α , while leaving the zero field spectrum unchanged. This effect is robust to a small asymmetry of the hopping amplitudes, which would make the Dirac cones anisotropic but would not change the structure of the LL spectrum [20]. We have related this unique behavior to a topological Berry phase which is no more π quantized. Contrary to the case of graphene, the valley degeneracy is broken by the magnetic field as soon as $\alpha \neq 0, 1$. We have provided a lattice model where the orbital response is affected in the whole energy spectrum, satisfying a fundamental sum rule, so that the responses at zero and finite dopings are systematically reversed.

Such an α - \mathcal{T}_3 model can be realized experimentally with cold fermionic atoms loaded in an optical lattice. Following the proposal of [21] for the optical dice lattice ($\alpha = 1$), one simply needs to dephase one of the three pairs of laser beams to obtain $\alpha \neq 1$ [15]. Simulating a perpendicular magnetic field by an artificial gauge potential [22]—as has been done very recently to study Hofstadter’s spectrum [23,24]—the internal energy and the entropy of the trapped Fermi gas could be measured following the techniques of [25]. From the dependence of the free energy on the magnetic field, the sign change of the susceptibility as a function of α could be directly tested. See [26] for an alternative proposal of an optical dice lattice with artificial gauge potential. de Haas–van Alphen oscillations could also be measured [27].

We acknowledge help from G. M. Tia at an early stage of this work and useful discussions with the mesoscopists in Orsay.

* fuchs@lptmc.jussieu.fr

[1] A. H. Castro Neto, F. Guinea, N. M. R. Peres, K. S. Novoselov, and A. K. Geim, *Rev. Mod. Phys.* **81**, 109 (2009).

- [2] M. Sepioni, R. R. Nair, S. Rablen, J. Narayanan, F. Tuna, R. Winpenny, A. K. Geim, and I. V. Grigorieva, *Phys. Rev. Lett.* **105**, 207205 (2010).
- [3] J. W. McClure, *Phys. Rev.* **104**, 666 (1956).
- [4] B. Sutherland, *Phys. Rev. B* **34**, 5208 (1986).
- [5] J. Vidal, R. Mosseri, and B. Douçot, *Phys. Rev. Lett.* **81**, 5888 (1998).
- [6] L. Landau, *Z. Phys.* **64**, 629 (1930); R. Peierls, *Z. Phys.* **80**, 763 (1933).
- [7] H. Fukuyama, *Prog. Theor. Phys.* **45**, 704 (1971).
- [8] G. Gómez-Santos and T. Stauber, *Phys. Rev. Lett.* **106**, 045504 (2011).
- [9] S. G. Sharapov, V. P. Gusynin, and H. Beck, *Phys. Rev. B* **69**, 075104 (2004).
- [10] After rescaling, the lattice model has hopping parameters $t_{AB} = t/\sqrt{1+\alpha^2}$ and $t_{CB} = \alpha t_{AB}$.
- [11] D. Bercioux, D. F. Urban, H. Grabert, and W. Häusler, *Phys. Rev. A* **80**, 063603 (2009).
- [12] G. P. Mikitik and Yu. V. Sharlai, *Phys. Rev. Lett.* **82**, 2147 (1999).
- [13] J. N. Fuchs, F. Piéchon, M. O. Goerbig, and G. Montambaux, *Eur. Phys. J. B* **77**, 351 (2010).
- [14] E. Akkermans and G. Montambaux, *Mesoscopic Physics of Electrons and Photons* (Cambridge University Press, 2007), Chap. 14.
- [15] See Supplemental Material at <http://link.aps.org/supplemental/10.1103/PhysRevLett.112.026402> for a derivation of the grand potential, a proof of the susceptibility sum rule and a proposal for an α - \mathcal{T}_3 optical lattice.
- [16] L. S. Gradshteyn and L. M. Ryzhik, *Table of Integrals, Series, and Products*, edited by A. Jeffrey (Academic Press, New York, 1994), 5th ed.
- [17] H. K. Nguyen and S. Chakravarty, *Phys. Rev. B* **65**, 180519 (2002), and references therein.
- [18] R. Rammal, *J. Phys. (Paris)* **46**, 1345 (1985).
- [19] Y. Ominato and M. Koshino, *Phys. Rev. B* **87**, 115433 (2013); see also J. Liu, Z. Ma, A. R. Wright, and C. Zhang, *J. Appl. Phys.* **103**, 103711 (2008).
- [20] M. O. Goerbig, J. N. Fuchs, G. Montambaux, and F. Piéchon, *Phys. Rev. B* **78**, 045415 (2008).
- [21] M. Rizzi, V. Cataudella, and R. Fazio, *Phys. Rev. B* **73**, 144511 (2006).
- [22] J. Dalibard, F. Gerbier, G. Juzeliunas, and P. Öhberg, *Rev. Mod. Phys.* **83**, 1523 (2011).
- [23] M. Aidelsburger, M. Atala, M. Lohse, J. T. Barreiro, B. Paredes, and I. Bloch, *Phys. Rev. Lett.* **111**, 185301 (2013).
- [24] H. Miyake, G. A. Siviloglou, C. J. Kennedy, W. C. Burton, and W. Ketterle, *Phys. Rev. Lett.* **111**, 185302 (2013).
- [25] Le Luo and J. E. Thomas, *J. Low Temp. Phys.* **154**, 1 (2009).
- [26] G. Möller and N. R. Cooper, *Phys. Rev. Lett.* **108**, 045306 (2012).
- [27] Ch. Grenier, C. Kollath, and A. Georges, *Phys. Rev. A* **87**, 033603 (2013).